THE JOURNAL OF BIOLOGICAL CHEMISTRY
Vol. 278, No. 3, Issue of January 17, pp. 1794–1801, 2003

Printed in U.S.A.

NUDT9, a Member of the Nudix Hydrolase Family, Is an Evolutionarily Conserved Mitochondrial ADP-ribose Pyrophosphatase*

Received for publication, June 5, 2002, and in revised form, October 16, 2002
Published, JBC Papers in Press, November 8, 2002, DOI 10.1074/jbc.M205601200

Anne-Laure Perraud‡, Betty Shen§, Christopher A. Dunn¶, Karsten Rippe‖, Megan K. Smith, Maurice J. Bessman¶, Barry L. Stoddard§, and Andrew M. Scharenberg‡****

From the ‡Department of Pediatrics, University of Washington and Children's Hospital and Regional Medical Center, Seattle, Washington 98195, the ¶Department of Biology, Johns Hopkins University, Baltimore, Maryland 21218, the §Division of Basic Sciences, Fred Hutchinson Cancer Center, Seattle, Washington 98109, and the ‖Deutsches Krebsforschungszentrum, Biophysik der Makromoleküle (H0500), Im Neuenheimer Feld 280 D-69120 Heidelberg, Germany

We have recently characterized the protein product of the human NUDT9 gene as a highly specific ADP-ribose (ADPR) pyrophosphatase (1). We now report an analysis of the human NUDT9 gene and its potential alternative transcripts along with detailed studies of the enzymatic properties and cell biological behavior of human NUDT9 protein. Our analysis of the human NUDT9 gene and twenty-two distinct cloned NUDT9 transcripts indicates that the full-length NUDT9α transcript is the dominant form, and suggests that an alternative NUDT9β transcript (2) occurs as the result of a potentially aberrant splice from a cryptic donor site within the first exon to the splice acceptor site of exon 2. Computer analysis of the predicted protein of the NUDT9α transcript identified an N-terminal signal peptide or subcellular targeting sequence. Using green fluorescence protein tagging, we demonstrate that the predicted human NUDT9α protein is targeted highly specifically to mitochondria, whereas the predicted protein of the NUDT9β transcript, which is missing this sequence, exhibits no clear subcellular localization. Investigation of the physical and enzymatic properties of NUDT9 indicates that it is functional as a monomer, optimally active at near neutral pH, and that it requires divalent metal ions and an intact Nudix motif for enzymatic activity. Furthermore, partial proteolysis of NUDT9 suggests that NUDT9 enzymes consist of two distinct domains: a proteolytically resistant C-terminal domain retaining essentially full specific ADPR pyrophosphatase activity and a proteolytically labile N-terminal portion that functions to enhance the affinity of the C-terminal domain for ADPR.

Free ADP-ribose (ADPR)[1] is a potentially toxic metabolite (reviewed in Ref. 3), and in addition has recently been demonstrated to act as a gating molecule for the TRPM2 ion channel (1), suggesting that it may have a signaling function in certain contexts. Production of free ADP-ribose occurs via a variety of pathways, and it is not presently clear which of these is most important *in vivo*. However, the catabolism of free ADP-ribose is thought to occur via a single pathway, hydrolysis to AMP and ribose-5-phosphate via ADP-ribose pyrophosphatases (ADPRases) (4–7). In humans, four distinct ADPRase activities have been described including three cytosolic activities (ADPRase-I, -II, and -Mn) and the mitochondrial ADPRase-m (4, 6, 7) based on traditional protein purification approaches. In contrast, cDNA cloning and characterization has identified only two human proteins, designated NUDT5 and NUDT9, respectively, having ADPRase activity (1, 8). NUDT5 is a cytosolic enzyme catalyzing the hydrolysis of ADP-ribose and other ADP-sugar conjugates (8). It appears to correspond to the previously described ADPRase-II based on the similarities of their reported substrate ranges. To date, NUDT9 has been shown to be highly specific for ADP-ribose, but has otherwise not been characterized in detail (1).

Here, we report the characterization of the human NUDT9 gene and its potential for alternative splicing and results from analyses of the physical, enzymatic, and cell biological properties of human NUDT9. Our results indicate that NUDT9α represents the previously characterized ADP-ribose-m, and provide insight into NUDT9 structure/function relationships as well as the relationship between NUDT9 proteins and a highly homologous domain (NUDT9H) of the TRPM2 calcium-permeable cation channel.

MATERIALS AND METHODS

cDNA Cloning and Sequence Analyses—Human cDNA transcripts were isolated as previously described from a spleen cDNA library (1). BLAST alignments were performed using the NCBI BLAST server. Computer analysis of sorting signals was performed using the PSORT and iPSORT algorithms available at the GenomeNet site in Japan. All other analyses and ClustalW alignments were performed using the MacVector program (Oxford Biotechnology). Clustal tree analysis was calculated using the nearest neighbor method with an open gap penalty of 10.0, extend gap penalty of 0.1, delay divergent of 40%, gap distance of 8, and a Block's substitution matrix similarity matrix.

Analysis of the human NUDT9 genomic structure was performed by aligning the NUDT9 mRNA sequence with the working draft of chromosome 4 available from GenBank™ and comparing the aligning regions with the predicted exons from the annotated version of chromosome 4 (exons were predicted by Genomescan). The exons based on alignment closely corresponded to those in the annotated sequences, with the primary exception that the first exon based on alignment starts 20 base pairs downstream of that predicted by Genomescan. Based on these approaches, the actual exons and corresponding bases in NUDT9 would be assigned as: exon1 = 6942506–6942100 (base pairs

* This work was supported by National Institutes of Health Grants GM64091 (to A. M. S.) and GM18649 (to M. J. B.). The costs of publication of this article were defrayed in part by the payment of page charges. This article must therefore be hereby marked "*advertisement*" in accordance with 18 U.S.C. Section 1734 solely to indicate this fact.

** To whom correspondence should be addressed: Dept. of Pediatrics, University of Washington and Children's Hospital and Regional Medical Center, 1959 NE Pacific Ave., Seattle, WA 98195. Tel.: 206-221-6446; Fax: 206-221-5469; E-mail: andrewms@u.washington.edu.

[1] The abbreviations used are: ADPR, ADP-ribose; ADPRase, ADP-ribose pyrophosphatases; MALDI-TOF, matrix-assisted laser desorption/ionization-time of flight; GFP, green fluorescence protein; EGFP, enhanced green fluorescence protein; WT, wild type; hum, human.

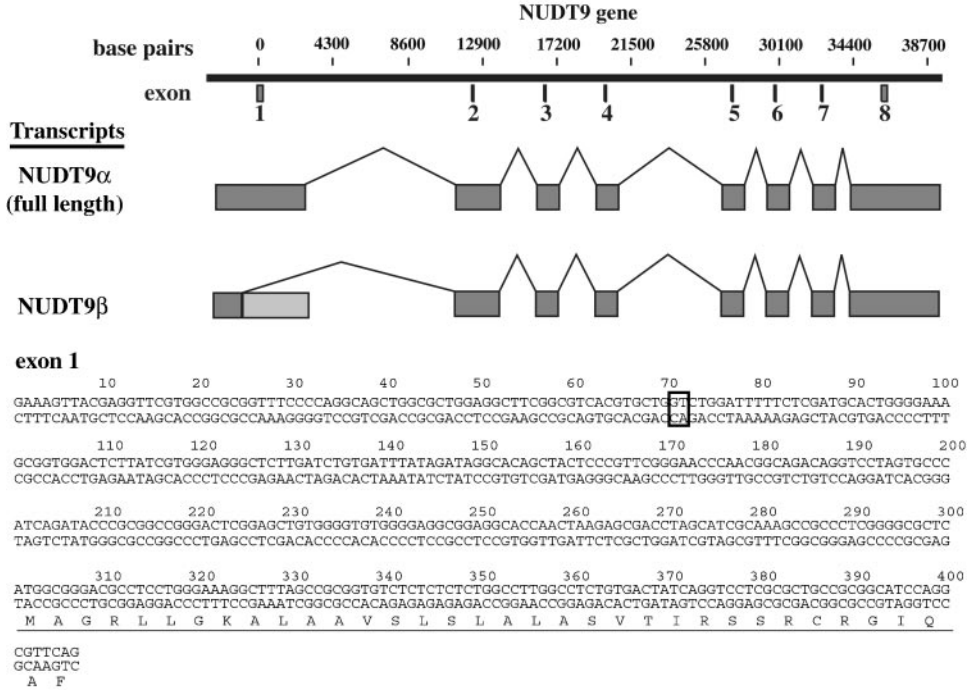

FIG. 1. **Organization of the NUDT9 gene and splicing of NUDT9*α* and NUDT9*β* transcripts.** The *light gray* portion of exon 1 in the splicing schematic for the NUDT9*β* transcript denotes the portion that is spliced out of NUDT9*β* in addition to the large first intron. The *black box* at base pair 70 of exon 1 denotes the apparent cryptic splice donor site within exon 1.

26–432 of the NUDT9 mRNA), exon 2 = 6930131–6929892 (base pairs 433–672 of the NUDT9 mRNA), exon3 = 6925969–6925874 (base pairs 673–768 of the NUDT9 mRNA), exon4 = 6922417–6922331 (base pairs 769–855 of the NUDT9 mRNA), exon5 = 6915104–6914993 (base pairs 856–965 of the NUDT9 mRNA), exon6 = 6912657–6912511 (base pairs 966–1114 of the NUDT9 mRNA), exon7 = 6909875–6909791 (base pairs 1115–1199 of the NUDT9 mRNA), and exon8 = 6906403–6905901 (base pairs 1200–1704 of the NUDT9 mRNA). Genomic base pair designations are for Homo sapiens chromosome 4 working draft sequence segment NT_006204.11 Hs4_6361.

Construction of Escherichia coli Expression Constructs for NUDT9α and NUDT9-H Region of TRPM2—Full-length coding sequences for NUDT9*α* and NUDT9*β* were produced by PCR to place an *Nco*I site at the 5′ end of the coding sequence and a *Not*I site at the 3′ end, and subcloned into the pET-24d T7 expression vector (Novagen). For the TRPM2 NUDT9 homology region, a construct was made by PCR to include a *Bsp*HI site, an artificial start codon, amino acids 1197–1503, a stop codon, and a 3′ *Not*I site. This was also subcloned into pET-24d. Other mutant forms of NUDT9 (see figure legends) were constructed using site-directed mutagenesis (QuikChange, Stratagene) of the NUDT9/pET-24d construct. Correct sequences of all constructs were confirmed by DNA sequencing.

E. coli Expression and Purification of NUDT9 and the NUDT9 Homology Region of TRPM2 and Assays for Nudix-type Activity of NUDT9 and NUDT9-H Region of TRPM2—Performed as previously described (1).

Analytical Ultracentrifugation—Analytical ultracentrifugation experiments were carried out on a Beckmann Instruments Optima XL-A with absorbance optics. Protein solutions of A_{280} = 0.21–0.42 (corresponding to a concentration of 3–6 μM in terms of protein monomer) were centrifuged at 20 C°. The buffer solution contained 50 mM Tris-HCl, pH 7.5, 50 mM KCl, and 0.1 mM dithiothreitol. The effect of Mg^{2+} was studied by supplementing the buffer with $MgCl_2$ to a concentration of 5 mM. For the NudT9 protein the following parameters were derived with the program SEDNTERP version 1.05 (J. Philo, D. Hayes, T. Laue; freely downloadable at alpha.bbri.org/rasmb/spin/ms_dos/) from the amino acid sequence: molecular mass of M_r = 36.2 kDa, extinction coefficient at 280 nm ϵ_{280} = 67050 $M^{-1}\cdot cm^{-1}$, partial specific volume $\bar{v}$ = 0.728 $ml\cdot g^{-1}$ at 20 °C, and a hydration of 0.44 g H_2O/g protein. The same program was used to calculate the buffer density and viscosity at 20 °C yielding ρ = 1.0020 $g\cdot ml^{-1}$ and η = 1.0124 milli-Pascal sec (buffer without $MgCl_2$) or ρ = 1.0024 $g\cdot ml^{-1}$ and η = 1.0126 milli-Pascal sec (buffer with 5 mM $MgCl_2$), and for modeling the apparent dimensions of an oblate or prolate including hydration according to the Teller method. Sedimentation equilibrium runs were conducted at 10,000 and 25,000 rpm. Equilibrium was reached after about 20 h of centrifugation as judged from comparison of successive scans. The baseline offset between sample and buffer was determined from the absorbance of the region close to the meniscus after sedimenting the protein sample at 48,000 rpm for 6 h. Equilibrium data were evaluated by fitting to a single exponential function as described previously (9). The sedimentation velocity data were recorded at 42,000 rpm using a spacing of 0.01 cm with four averages in the continuous scan mode. Data were analyzed by computing the sedimentation coefficient distribution (g(s*)) distribution (10, 11) with the program DCDT+ version 1.13 by John Philo according to the algorithm described (12).

Partial Proteolysis of Nudt9 and Subsequent Analysis of the Obtained Fragments—A serial dilution from a 1 mg/ml stock solution of the nonspecific cysteine protease bromelain (Calbiochem) was made, and the appropriate protease concentration for the partial proteolysis of purified Nudt9 (0.75 mg/ml final) was determined. A final bromelain concentration between 0.75 and 6.25 μg/ml in the protease reaction (60′ incubation at 37 °C) gave a clear and reproducible pattern showing one main subfragment around 20 kDa. The time course analysis of the protease reaction was performed using a 1.56 μg/ml final concentration of bromelain. The reaction mixture contained beside the proteins, 25 mM Tris, pH 7.5, 100 mM NaCl, 1 mM $MgCl_2$, and 1 mM dithiothreitol. The reactions were stopped by the addition of a 10-fold excess of iodoacetamide followed by SDS-PAGE. Two stable fragments from the Coomassie-stained gel were subjected to MALDI-TOF mass spectroscopic analysis in a Bruker Daltonic Spectrometer (Billerica, MA) operated in the reflectron mode. Spectra were externally calibrated with a standard peptide mixture and analyzed using the program "*m/z*" from Proteometrics (Winnipeg, Manitoba). Coomassie-stained gel bands were digested in-gel with trypsin (omitting reduction and alyklation). Following overnight digestion, the digestion buffer was removed from the gel slices and trifluoroacetic acid was added to a final concentration of 0.5%. A 5-μl fraction of the digestion mixture was concentrated and purified using a nano-scale column and column elution was accomplished with the matrix solution (0.1% trifluoroacetic acid/50% acetonitrile saturated with alpha-cyano-4-hydroxycinammic acid) onto the MALDI target.

To determine the N-terminal residues of the obtained main fragment the partial proteolysis reaction was separated by SDS-PAGE in a 12.5% polyacryalmaide gel and transferred to a polyvinylidene difluoride membrane (Millipore). The obtained protein bands were stained by Coomassie and excised for further analysis by Erdman-degradation chemistry.

Eukaryotic Expression of NUDT9—Wild type human NUDT9*α* and NUDT9*β* cDNAs were subcloned to pCDNA4/T0, transfected into either tet-supressor expressing DT-40 B-cells or HEK-293 cells by electropo-

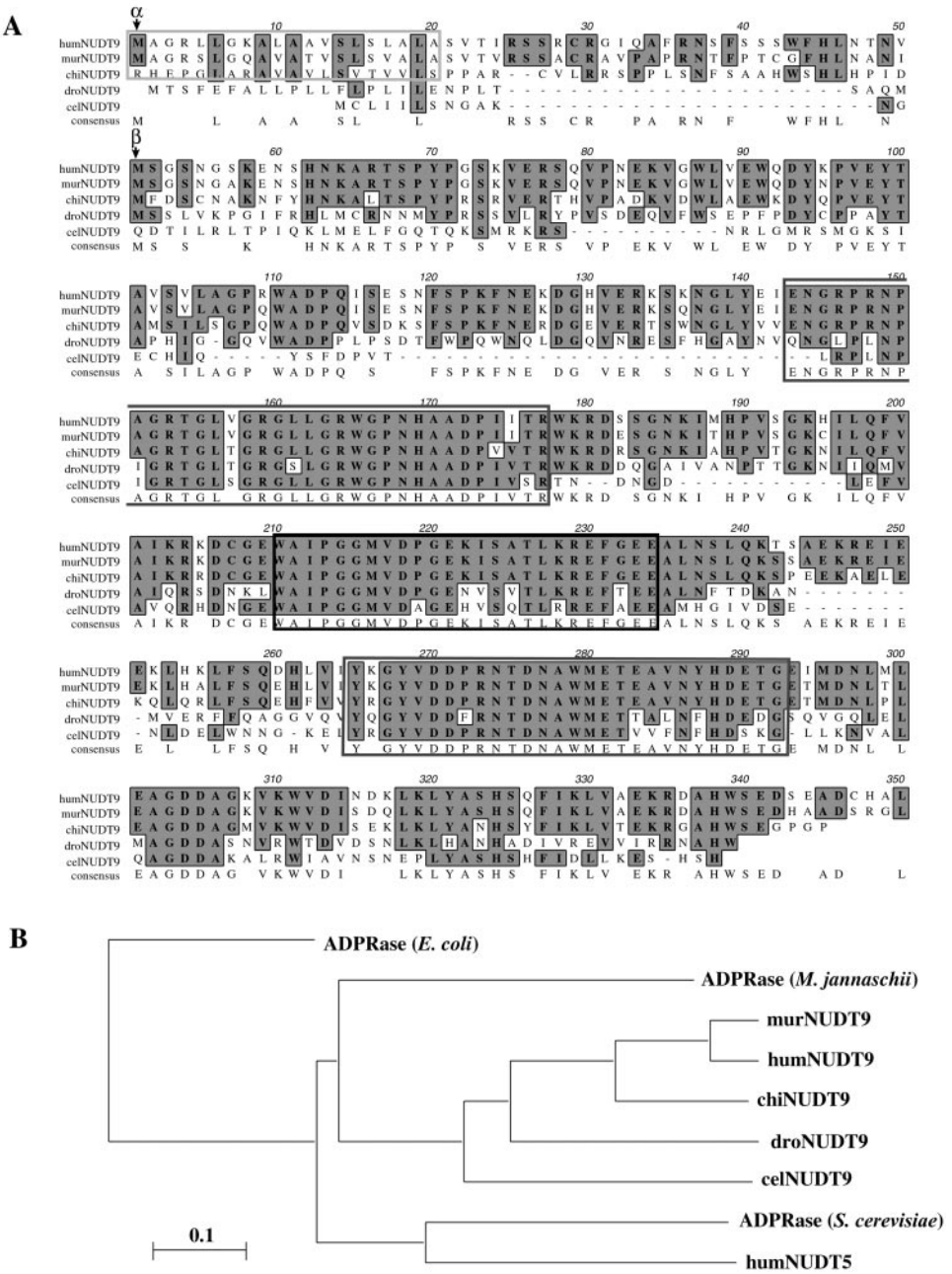

FIG. 2. **Alignment and phylogenetic analysis of NUDT9 homologs.** *A*, alignment of various species of NUDT9 homologs. Alignment was performed using ClustalW. α and β denote the initiating methionines of the NUDT9α and NUDT9β proteins, respectively. *B*, phylogenetic relationship of NUDT9 homologs and four other examples of Nudix family ADPRases. The evolutionary tree was calculated using the neighbor joining method. Evolutionary distance is shown by the total branch length (*horizontal lines*).

ration, and zeocin-resistant clones were isolated. Cells untreated with tetracycline showed no detectable protein expression, whereas treated cells produced the level of protein expression illustrated in Fig. 4*A*. A NUDT9α-EGFP fusion protein was constructed by placing a *Kpn*I site internal to the NUDT9 stop codon and ligating this to an EGFP (Clontech) construct containing a *Kpn*I site placed just internal to the start codon. This construct was ligated into the *Not*I and *Xho*I sites of the pCDNA4/TO vector (Invitrogen). The NUDT9α-EGFP in pCDNA4/T0 was transfected into HEK-293 cells and DT-40 cells expressing the tet-repressor, and zeocin-resistant clones were isolated. Cells untreated with tetracycline showed no detectable protein expression, whereas treated cells were obviously fluorescent and showed the staining patterns illustrated in Fig. 4*B*.

Protein Analysis—Typically cells were lysed at 5×10^6 cells per ml of lysis buffer, and lysates were cleared by centrifugation at 14,000 RPM for 15 min prior to preparation for SDS-PAGE. SDS-PAGE and immunoblotting were performed using standard techniques. Anti-NUDT9 antibody was generated by immunizing rabbits with a peptide DDPRNTDNAWMETEAVNYHDETGE, corresponding to amino acids 270–293 near the C terminus of the enzyme.

Fluorescence Imaging—Cells expressing NUDT9α-GFP and NUDT9β-GFP fusion proteins were plated on cover slips and digitally imaged at 40× magnification. The conditions used produced no detectable fluorescence from uninduced cells. For co-localization experiments, mitochondria and nuclei were separately stained with Mito-Tracker dye and Hoechst 33342 (Molecular Probes), respectively. Using conditions in which no bleed through was detected from Mito-Tracker or Hoechst staining into GFP channels, images of NUDT9α-GFP, Mito-Tracker, and Hoechst staining were separately collected using filter sets specific for each dye, respectively.

RESULTS

Computer Analysis of the Human NUDT9 Gene—The NUDT9 gene is located on chromosome 4 as previously reported by Lin *et al.* (2), who also reported the presence of two

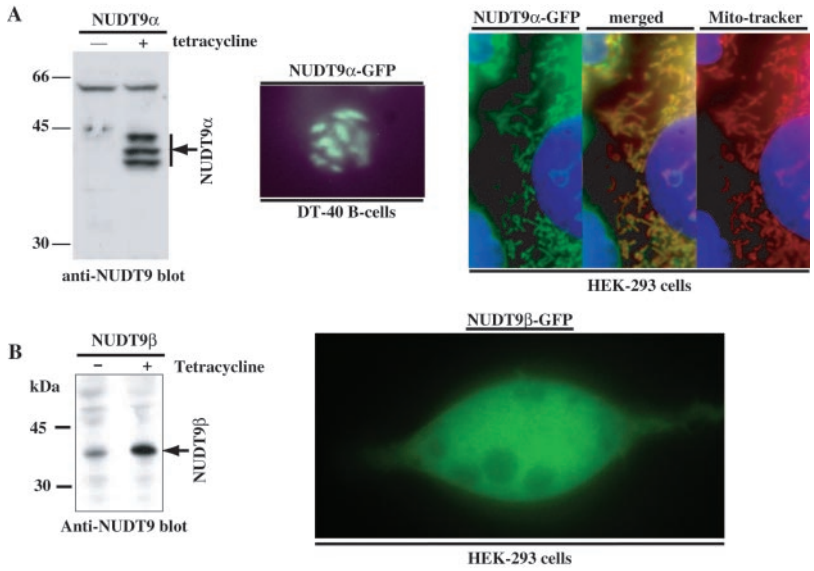

FIG. 3. **Eukaryotic expression and subcellular localization of NUDT9.** *A*, eukaryotic expression of NUDT9α. *Left panel*, a human NUDT9α expression construct was transfected as described under "Materials and Methods" and analyzed by SDS-PAGE and immunoblotting with an anti-NUDT9 antibody. *Middle panel*, localization of NUDT9α-GFP in chicken DT-40 B-cells. Chicken DT-40 B-cells were transfected with a NUDT9α-GFP fusion protein construct, and the subcellular localization of this construct was imaged as described under "Materials and Methods." *Right panel*, HEK-293 cells were transfected with a NUDT9α-GFP fusion protein construct, and the subcellular localization of this construct (*green*), cellular mitochondria (*red*), and nuclei (*blue*) were imaged separately as described under "Materials and Methods." *B*, eukaryotic expression of NUDT9β. *Left panel*, a human NUDT9β expression construct was transfected as described under "Materials and Methods" and analyzed by SDS-PAGE and immunoblotting with an anti-NUDT9 antibody. *Right panel*, HEK-293 cells were transfected with a NUDT9β-GFP fusion protein construct, and the subcellular localization of this construct was imaged as described under "Materials and Methods."

NUDT9 transcripts designated NUDT9α and NUDT9β (nomenclature that we will adhere to for both the transcripts and specific proteins for this report, whereas when referring to enzymatic activity we will simply refer to NUDT9). Based on comparison of the NUDT9α and NUDT9β cDNAs, Lin *et al.* (2) suggested that the NUDT9 primary transcript is alternatively spliced to produce these two transcripts via inclusion of an intron in the longer NUDT9α transcript. However, their study did not include an analysis of the NUDT9 genomic structure. We have analyzed the structure of the human NUDT9 gene using sequences available from public databases (Fig. 1), and our analysis indicates that the NUDT9 gene consists of 8 well defined exons spread over ~37 kb. Based on this gene structure, the NUDT9β variant transcript is not produced by removal of an intron but is instead the result of a potentially aberrant splice from a splice donor within the first NUDT9 exon to the splice acceptor site at the beginning of exon 2. This conclusion is based on: 1) the presence of the entire putative exon 1 as defined here in the reported NUDT9α transcript; 2) the presence of the entire putative exon1 as defined here as a contiguous sequence within the present chromosome 4 working draft sequence; and 3) the presence of a large (>10 kb) well defined intron adjacent to exon 1, which is spliced from both the NUDT9α and NUDT9β transcripts. As a means of assessing the relative abundance of NUDT9α and NUDT9β transcripts, we end-sequenced twenty-two separate NUDT9 clones that had been isolated utilizing a selection cloning method targeting sequences between base pairs 597 and 849 of the NUDT9α transcript (thereby targeting sequences contained within exons 2 and 3, such that both NUDT9α and NUDT9β transcripts would be isolated). Of these twenty-two clones, eighteen contained either full-length or nearly full-length transcripts corresponding to NUDT9α. Of the four transcripts with alternative 5′ ends, two were truncated within exon 1 after the start of the predicted NUDT9α coding sequence, one was truncated at the end of exon 2, and one represented the previously reported NUDT9β transcript. These results indicate that in human spleen, the tissue from which our NUDT9 sequences were cloned, the NUDT9α transcript is by far the dominantly expressed transcript. Determining the question of whether there is any physiological relevance of NUDT9β or if it simply represents a low abundance aberrant transcript will require investigation into whether there are proteins in the native tissue corresponding to the predicted product of the NUDT9β transcript. This task will be complicated by the fact that NUDT9α is extensively processed (see below) leading to the production of proteins extremely close in size to that of the protein predicted to be encoded by NUDT9β.

An alignment of the predicted NUDT9α protein sequences from several organisms is shown in Fig. 2*A*. As can be seen, NUDT9 is highly conserved, with >60% identity and ~80% similarity at the amino acid level. BLAST alignments of the human, mouse, and chicken sequences with various NCBI databases identified close homologs in *Drosophila melanogaster* (droNUDT9 in Fig. 2A) and *Caenorhabditis elegans* (celNUDT9 in Fig. 2*A*) based on the presence of the conserved Nudix box (*black outline box*) and highly conserved regions both upstream and downstream from it (*dark gray outline boxes*). Interestingly, these analyses failed to identify significantly related sequences in any prokaryote or unicellular eukaryote. Computer analysis of the N-terminal 100 amino acids of human NUDT9α using PSORT and iPSORT had previously demonstrated the presence of a conserved putative signal peptide or subcellular compartment targeting presequence (1). Similar analyses of murine NUDT9α gave identical results. Although the chicken NUDT9α sequence is not yet complete, it appears that the signal peptide/targeting presequence is present in the chicken version as well based on the degree of conservation of this region relative to that of human and murine NUDT9α predicted proteins. This suggests that vertebrate NUDT9 homologs are all likely to be either secreted or subcellularly compartmentalized. Computer analyses of the N termini of either droNUDT9 or celNUDT9 did not predict the presence of a signal peptide or subcellular targeting presequence, although the degree of aliphilicity of this region in both of these enzymes is suspicious for their functioning in this manner as well.

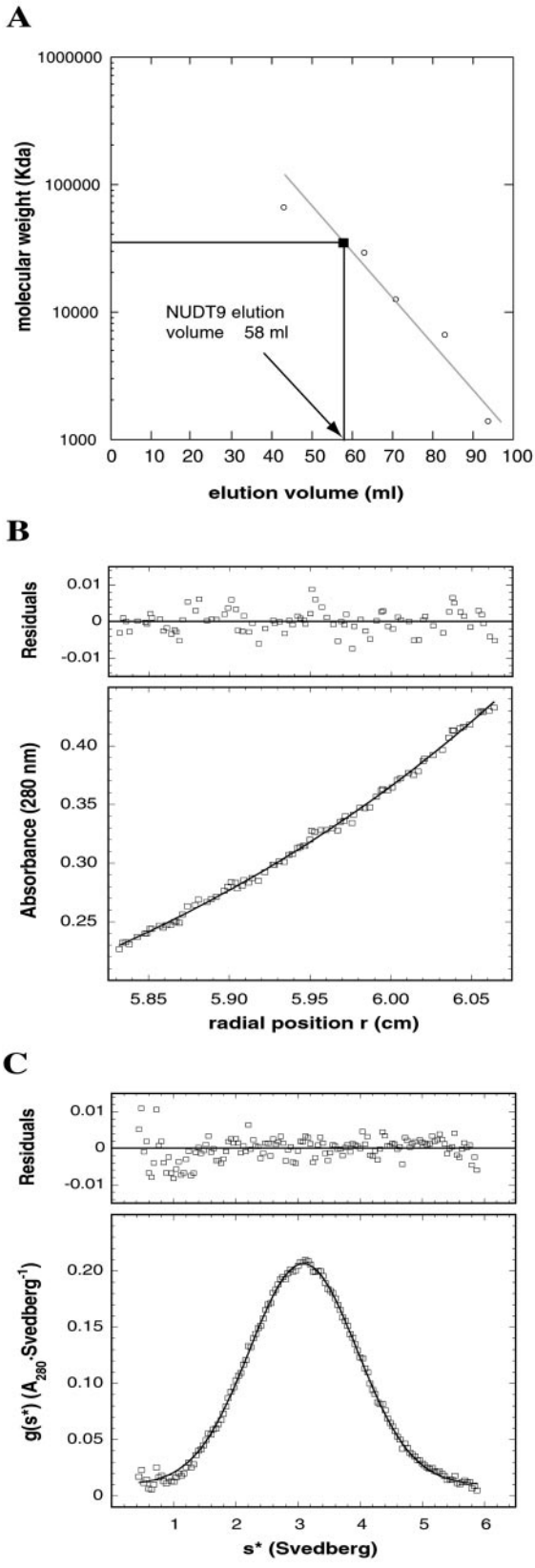

FIG. 4. **NUDT9 association state studied by gel permeation chromatography and analytical ultracentrifugation.** *A*, gel permeation chromatagraphy of NUDT9. NUDT9 protein was chromatographed on a Fractogel-EMD-Biosec column, and its elution volume was measured as 58 ml. Five standards used for column calibration (Vit B12, aprotinin, cytochrome C, carbonic anhydrase, and bovine serum albumin) are plotted with NUDT9 on the *right*. A regression line calculated using the known M_r of the standards and their measured elution volumes predicts a molecular mass of ~36 kDa for NUDT9. *B*, example of a sedimentation equilibrium run in Mg^{2+}-containing buffer of NUDT9 protein at a concentration of 6 μM and a rotor speed of 10,000 rpm. In the *bottom* part of the figure the measured absorbance at 280 nm *versus* the radial position (distance to the center of the rotor) is shown. The *top* part of the figure gives the residuals to the fit expressed as the difference between experimental and fitted values. Only every third data point is shown. For the data presented in this figure a molecular mass of 38.0 kDa was determined. All equilibrium data recorded at different concentrations and two rotor speeds gave an average molecular mass of M_r = 38.9 ± 2.5 kDa. *C*, sedimentation velocity run of NUDT9 analyzed by the $g(s^*)$ method in Mg^{2+}-containing buffer. The fit curve corresponds to a sedimentation coefficient of $s_{20,w}$ = 3.1 S (maximum of the distribution) and a diffusion constant of $D_{20,w} = 7.4 \cdot 10^{-7}$ cm^2 sec^{-1} determined from the width of the gaussian-shaped function. The molecular mass calculated from s and D in this experiment was M_r = 37 kDa.

The evolutionary relationship of the various NUDT9 homologs and four other proteins with ADPRase activity, NUDT5, *Saccharomyces cerevisiae* ADPRase, *E. coli* ADPRase, and *Methanococcus jannaschii* ADPRase, is summarized in a CLUSTAL phylogenetic tree graph (Fig. 2*B*). Based on this analysis, *E. coli* ADPRase and NUDT5 and the *S. cerevisiae* ADPRase appear to represent families distinct from a well defined family containing the various NUDT9 homologs, consistent with the broader substrate specificities of these three enzymes (5, 8, 13). In contrast, the *M. jannaschii* ADPRase is grouped more closely to the NUDT9 family, consistent with its high degree of specificity for ADP-ribose and the similarity of its metal ion requirements to those of NUDT9 (Ref. 14 and see below). Whether the degree of similarity observed between the *M. jannaschii* (an *Archae*on) enzyme and the NUDT9 family is due to divergent or convergent evolution is not presently clear. As more full organism genomes become available for analysis, greater insight into the evolutionary relationship of highly specific ADPRases may be possible.

Analysis of NUDT9α and NUDT9β Subcellular Localization—As discussed above and as illustrated in Fig. 2 (*light gray outline box*), all vertebrate NUDT9 homologs have an apparent N-terminal signal peptide/targeting signal in their major transcripts (designated NUDT9α), which is potentially missing in the NUDT9β variant transcript. To investigate what role this sequence might play during NUDT9α biosynthesis, we transfected DT-40 B-cells or HEK-293 cells with NUDT9α and NUDT9β cDNAs and analyzed NUDT9α expression by immunoblotting with an anti-NUDT9 antibody (Fig. 3). NUDT9α transfection induced the appearance in cell lysates (but not in the culture supernatants) of three new bands in the 30–40 kDa molecular mass range (Fig. 3*A*, *left panel*, the small *blips* at 45 kDa in the uninduced lane appear to represent spurious signal due to a slight defect in membrane blocking)). Identical results were obtained in HEK-293 cells (data not shown). We interpret the abundance of anti-NUDT9 immunoreactivity in cell lysates as most consistent with the NUDT9α N-terminal region acting as a sorting signal for subcellular compartmentalization as opposed to secretion, and the presence of three bands as most consistent with proteolysis of both the predicted NUDT9α signal peptide and a second sequence as well. Consistent with its lack of a predicted signal sequence, NUDT9β transfection (Fig. 3*B*, *left panel*) produced only a single NUDT9-immunoreactive band, presumably because it lacks the sequence proteolyzed or because the product of the NUDT9β transcript was not targeted to the compartment containing the requisite protease. To directly determine where the NUDT9α and NUDT9β protein products were subcellularly localized, we produced NUDT9α and NUDT9β C-terminal-EGFP fusion protein expression constructs and imaged their subcellular localization. As shown in Fig. 3*A* (*middle panel*), the NUDT9α-GFP fusion protein produced a compartmentalized staining pattern consistent with its

localization to mitochondria or other large organelle in DT-40 B-cells. Because DT-40 cells have little cytoplasm, they are not an optimal system for organellar marker co-localization studies. Therefore we used the same NUDT9α-GFP expression construct to transfect HEK-293 cells and imaged its subcellular localization in conjunction with specific staining of mitochondria with Mito-Tracker dye and nuclei with Hoechst 33342 (Fig. 3*A*, *right panel*). As can be seen, the NUDT9α-GFP fusion protein is visible in structures with a morphology highly characteristic of mitochondria and that stain specifically with the Mito-Tracker dye. The same pattern was observed when NUDT9α-GFP was expressed and imaged in the absence of Mito-Tracker staining (data not shown). In contrast (Fig. 3*B*, *right panel*), the NUDT9β C-terminal-EGFP fusion protein showed no apparent subcellular localization when expressed alone. From the above studies, we conclude that NUDT9α is produced as a precursor polypeptide and specifically imported into mitochondria where it undergoes a two step processing to its mature form, whereas NUDT9β is neither specifically compartmentalized nor further processed.

NUDT9 Association State Studied by Gel Permeation Chromatography and Analytical Ultracentrifugation—Many Nudix enzymes are dimers (15, 16), and recent structural data on the *E. coli* ADPRase indicate that it functions as a dimer (17), suggesting this might be the case for other members of the classical ADPRase family. To determine whether a similar mode of function applies to NUDT9, we analyzed the molecular weight of purified enzymatically active human NUDT9, which has a calculated molecular mass (M_r) of 39,121 daltons, by gel permeation chromatography and analytical ultracentrifugation. On gel permeation chromatography, NUDT9 eluted as a single sharp peak at ~60 ml elution volume, corresponding to $M_r \approx 40$ kDa based on our column calibration (Fig. 4*A*). The sharp peak and close correlation of calculated molecular mass with the molecular mass predicted from chromatographic behavior are strong evidence that, under the conditions used, NUDT9 is entirely monomeric in form.

We next studied the association state and hydrodynamic shape of NUDT9 by analytical ultracentrifugation. Fig. 4*B* shows an example of a sedimentation equilibrium run of NUDT9 protein, whereas Fig. 4*C* displays the analysis of a sedimentation velocity experiment by the $g(s^*)$ method (10, 11). Both runs were conducted in Mg^{2+}-containing buffer. In the absence of $MgCl_2$, the sedimentation properties of the proteins remained unchanged (data not shown). The average molecular weight determined from the sedimentation equilibrium runs of multiple samples at different protein concentrations and examined at two rotor speeds was $M_r = 38.9 \pm 2.5$ kDa. In the sedimentation velocity analysis a sedimentation coefficient of $s_{20,w} = 3.1 \pm 0.1$ S (maximum of the distribution) and a diffusion constant of $D_{20,w} = (7.4 \pm 0.5) \cdot 10^{-7}$ cm^2 sec^{-1} determined from the width of the distribution were obtained. These values of s and D correspond to a molecular mass of 37 ± 4 kDa as calculated according to the Svedberg equation. Based on the above analyses, we conclude that, in contrast to the bacterial ADPR pyrosphosphatase, NUDT9 is likely to be active in monomeric form. With an estimated hydration of 0.44 g H_2O/g protein for NudT9 the ratio of the measured friction coefficient f (calculated from s and M) to that of a sphere with the same volume f_0 was $f/f_0 = 1.10$. The corresponding axial ratios for the hydrodynamic dimensions of the protein are 2.8 assuming a disk-shaped oblate (7.3 diameter and 2.6 nm height) and 2.7 for a rod-like prolate (10.1 length and 3.7 nm diameter), indicating that the shape of NUDT9 in solution deviates significantly from that of a sphere.

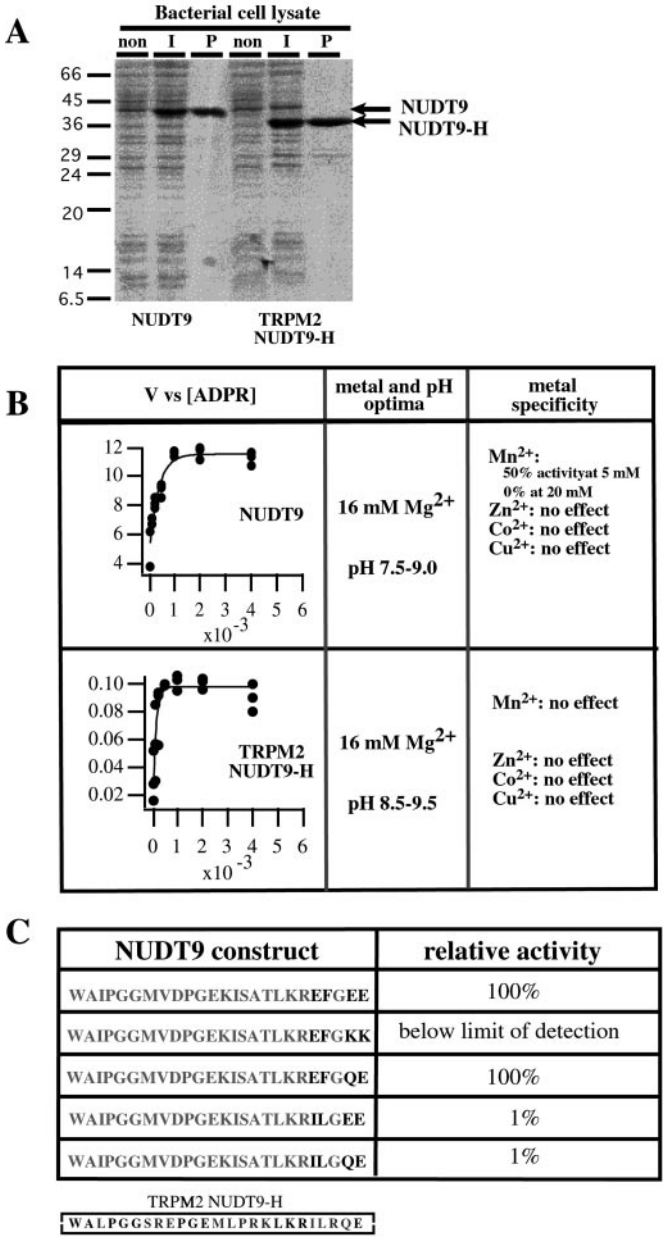

FIG. 5. **Purification and analysis of NUDT9 activity.** *A*, purification of NUDT9 and NUDT9H. Shown are Coomassie-stained gels of lysates of bacteria expressing NUDT9 (*left panel*) or the TRPM2 NUDT9-H (*right panel*) before induction (*non*), after induction (*I*), and after subsequent purification (*P*). *B*, Michaelis-Menten plots, metal-ion and pH optima, and metal-ion specificity of NUDT9 and NUDT9-H. *C*, mutational analysis of NUDT9 activity. Shown in the *table* are the amino acid sequences of the Nudix motif (*left column*) and the measured enzymatic activity at saturating [ADPR] (*right column*) of various NUDT9 constructs. The first construct is wild type NUDT9; the structure of the TRPM2 Nudix motif is shown in the *box* just below the *table*.

Metal Ion and Mutational Analysis of the Role of the Nudix Motif in NUDT9 ADPR-pyrophosphatase Activity—We have previously reported an initial characterization of NUDT9 and the isolated TRPM2 NUDT9-H domain as specific ADPRases (1). As a member of the Nudix family, it would be expected that NUDT9 enzymatic activity is dependent on the presence of metal ions and an intact Nudix motif (15, 16). To experimentally verify the dependence of NUDT9 catalytic activity on metal ions, we produced NUDT9 and the TRPM2 NUDT9-H in bacteria and purified them to homogeneity (Fig. 5*A*, *left panel*). Analysis of their respective activities under standard conditions produced the Michaelis-Menten plots shown in Fig. 5*B*,

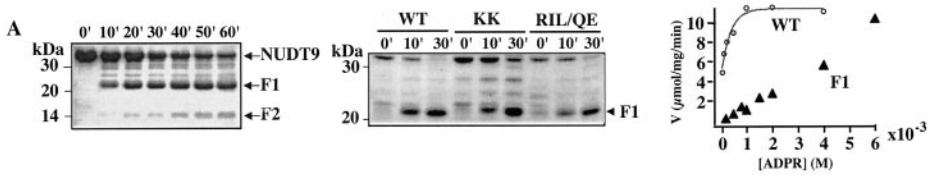

B

```
MAGRLLGKAL AAVSLSLALA SVTIRSSRCR GIQAFRNSFS SSWFHLNTNV MSGSNGSKEN   60
SHNKARTSPY PGSKVERSQV PNEKVGWLVE WQDYKPVEYT AVSVLAGPRW ADPQISESNF  120
SPKFNEKDGH VERKSKNGLY EIENGRPRNP AGRTGLVGRG LLGRWGPNHA ADPIITRWKR  180
DSSGNKIMHP VSGKHILQFV AIKRKDCGEW AIPGGMVDPG EKISATLKRE FGEEALNSLQ  240
KTSAEKREIE EKLHKLFSQD HLVIYKGYVD DPRNTDNAWM ETEAVNYHDE TGEIMDNLML  300
EAGDDAGKVK WVDINDKLKL YASHSQFIKL VAEKRDAHWS EDSEADCHAL              350
```

FIG. 6. **Partial proteolysis of purified wild type and mutant NUDT9 proteins.** *A*, *left panel*, time course of the partial proteolysis of purified WT NUDT9 with the protease bromelain, using 15 μg NUDT9 and 30 ng bromelain per lane. The obtained subfragments are designated F1 and F2. *Middle panel*, time course of proteolysis of WT NUDT9 and point mutants mutants KK and RIL/QE using the same conditions as for *A*. *Right panel*, V *versus* S plot for activity of wild type NUDT9 (*line with circles*, averaged data from Fig. 2) and purified recombinant F1 subfragment (*triangles*). *B*, results of the mass-spectrometric analysis of the obtained subfragments F1 and F2 shown under *A* by MALDI mass spectrometry. Identified peptides after in-gel trypin digestion of the F1 and F2 fragments are *underlined* in *dark gray* (*F1*) or light gray (*F2*), demonstrating that F2 is a degradation fragment of F1. The *black arrow* shows the N terminus of the F1 fragment as determined by Edman-degradation chemistry of the western-blotted F1 fragment.

left panels (K_m and V_{max} from these plots were previously reported in Ref. 1), and metal and pH optima and metal specificities derived from ion or pH manipulations performed at saturating [ADPR] (2 mM) are shown in the *right* and *middle panels*. As can be seen, both enzymes have maximal activity at 16 mM Mg^{2+} and in similar pH ranges, with NUDT9 but not the TRPM2 NUDT9-H having the ability to allow Mn^{2+} to substitute for 50% of maximal activity at 5 mM. To experimentally verify the role of the Nudix motif in NUDT9 catalytic activity, we performed a mutational analysis of Nudix motif critical residues (Fig. 5*C*). We first mutated the terminal EE residues of the Nudix motif of NUDT9 to lysines, produced the protein in *E. coli*, purified it as for wild type NUDT9, and assayed its enzymatic activity. The EE → KK substitutions eliminated detectable ADPRase activity, confirming the requirement for an intact Nudix motif in NUDT9 catalytic function. We had previously observed that although the TRPM2 NUDT9-H domain has ADPRase activity, it is two orders of magnitude lower than that of NUDT9 (1). We had therefore speculated that two Nudix motif substitutions found in the NUDT9-H of TRPM2 (REF → RIL and EE → QE) accounted for its markedly lower level of activity relative to NUDT9. To test the relevance of these substitutions, we produced NUDT9 versions with various combinations of the Nudix motif substitutions found in the TRPM2 NUDT9H, purified them, and assayed their activity at saturating [ADPR] (2 mM). The REF → RIL substitution greatly reduced detectable NUDT9 activity in our assay (to ~1% of wild type), whereas the EE → QE substitution caused little or no detectable change in activity of either wild type or RIL versions. We therefore conclude that the REF → RIL substitution found in the TRPM2 NUDT9-H is sufficient to account for the loss of activity of the NUDT9-H domain relative to NUDT9. The REF → RIL and EE → KK mutant enzymes were as stable as WT NUDT9 and easily purified, suggesting that they fold normally into a stable three-dimensional structure and that the effect of the mutations is due to alterations within or nearby the NUDT9 active site. This conclusion is further supported by results from partial proteolysis of these enzymes (see below).

Partial Proteolysis of WT NUDT9 and REF → RIL and EE → KK Mutant Enzymes Reveals a Core Enzyme with ADPRase Activity—Because site-directed mutagenesis of enzymes can produce altered protein folding, which hinders clear interpretation of the effects of a particular mutation on enzymatic activity, we compared partial proteolytic patterns of wild type, REF → RIL and EE → KK enzymes. All three enzymes gave an identical pattern consisting of the appearance of a major fragment (F1) of molecular mass 22 kDa (Fig. 6*A*, *left* and *middle panels*), suggesting that the mutant enzymes fold into the same basic conformation as WT NUDT9. We purified the F1 fragment for WT NUDT9, and obtained N-terminal and internal protein sequences from it (Fig. 6*B*, *underlined sequences*). These protein sequences identified the fragment as extending from residue 164 of the NUDT9 coding sequence to near the end of the predicted protein, including the Nudix motif where our mutations were targeted. An expression vector was constructed for the WT NUDT9 F1 fragment, and it was expressed and purified. Assays of this preparation of purified F1 fragment for ADPRase activity demonstrated that it retained a high degree of specificity (its activity toward the close ADPR homologue ATP remained undetectable) and had an identical V_{max} as compared with the wild type protein, although it had a significantly reduced K_m (see V (reaction velocity) *versus* S (substrate concentration) *plot*, Fig. 6*A*, *right panel*). That both WT and mutant enzymes produce the same proteolysis-resistant fragment and that this fragment retains specific ADPRase activity together provide strong support for the conclusion that the RIL and KK mutations alter NUDT9 activity by virtue of direct effects on the enzyme active site. The fact that the "core" C-terminal fragment retains both activity and specificity but has a substantially reduced K_m further suggests that NUDT9 is a multi-domain enzyme in which the N-terminal domain acts to enhance the binding affinity of NUDT9 for ADP-ribose, whereas the C-terminal domain provides catalytic specificity and activity. The N-terminal domain may in addition play other specialized regulatory functions. One such possibility is functioning as an interaction domain for targeting NUDT9 ADPRase activity to a specific microenvironment.

DISCUSSION

The analyses of NUDT9 reported here indicate that there are highly conserved NUDT9 homologs present in the most widely studied multicellular eukaryotic organisms, and that, in vertebrates at least, NUDT9 predominantly functions in monomeric form within mitochondria utilizing either Mg or Mn as a metal ion cofactor bound to the Nudix motif.

Several types of human ADPRases have been isolated based on procedures for purification of ADPRase activities from cell

and organellar extracts. One of these, designated ADPRase-m, has been purified from mitochondria and characterized in some detail (7). Several lines of evidence suggest that this enzyme is likely to be the protein product encoded by NUDT9α. First, mitochondria had ADPRase activity, which eluted as a single peak during ion exchange and size exclusion chromatography, suggesting that they contain only a single ADPRase enzyme (7). Second, the purified protein had a predicted molecular mass of 35 kDa (7), similar to the predicted molecular mass of 39,121 for NUDT9α, particularly given that the post-translational proteolytic processing observed for NUDT9α would reduce the size of the native enzyme isolated from mitochondria. Although the K_m reported for this enzyme was 2–3 μM, far lower than the 100 μM K_m we have observed for recombinant NUDT9 (1, 7), this may be due to differences in assay conditions or altered properties of the recombinant enzyme due to its not having undergone the same post-translational proteolytic processing as the endogenous enzyme. A 39-kDa cytosolic highly specific ADPRase (ADPRase-I) was also reported by this same group (18), which is significantly more than the 33 kDa size predicted for the product of the NUDT9β transcript or for the processed forms of NUDT9α. Determining whether ADPRase-I represents the product of the NUDT9β transcript, alternative translational initiation from a downstream methionine in full-length NUDT9α transcripts, partially/differentially processed NUDT9α, or the product of a gene other than NUDT9 will require further investigation.

Recent structural data from the *E. coli* ADPRase (17) indicate that it functions as a dimer in which the interacting surface of one subunit provides part of the substrate recognition surface for catalysis mediated by the active site of the other subunit. In contrast, our analyses suggest that NUDT9 is active as a monomer. This is consistent with the marked sequence divergence between NUDT9 and other classic ADPRases exemplified by the *E. coli*, *S. cerevesiae*, and human NUDT5 sequences included in the phylogenetic analysis of Fig. 1. Based on the presence of highly conserved regions on either side of the conserved Nudix catalytic site of NUDT9 (*dark gray boxed* areas in Fig. 1), it seems likely that interactions between ADPR and these regions of NUDT9 account for the high degree of enzymatic specificity exhibited by NUDT9. The results of the partial proteolysis, in which a core fragment from the C-terminal region of NUDT9 including these regions was found to retain substantial specific ADPRase activity also support this conclusion and furthermore suggest that NUDT9 has a proteolytically labile N-terminal domain, which enhances the affinity of the C-terminal domain for ADPR.

Our mutational analysis confirms the role of the Nudix motif in the ADPRase activity of NUDT9, and provides insight into the relationship between NUDT9 and the NUDT9-H domain found in TRPM2. We had previously speculated that the REF $\rightarrow$ RIL and EE $\rightarrow$ QE substitutions accounted for the decreased enzymatic activity of the NUDT9-H domain relative to NUDT9 (1). Our present mutational analysis suggests that the REF $\rightarrow$ RIL substitution is the most important determinant of the decreased activity, and that the EE $\rightarrow$ QE substitution would not substantially affect the activity of the TRPM2 NUDT9-H. As an additional point, previous work (19, 20) on Nudix motif mutations in the context of other NUDIX enzymes has suggested that mutation of the glutamate residue in the REF motif would eliminate metal-ion binding but otherwise leave the enzyme structure intact, an idea further supported by the *E. coli* ADPRase structure, where the Nudix motif is positioned for involvement in catalysis but not substrate recognition. These observations add credence to the hypothesis that the NUDT9-H of TRPM2 is an evolutionary adaptation of NUDT9 as an interaction domain for ADPR-mediated gating of TRPM2.

The demonstration that human NUDT9 is to a large extent likely to be compartmentalized specifically to mitochondria, the high level conservation among vertebrate NUDT9 homologs of the signal sequence most likely involved in mitochondrial targeting of NUDT9, and the observation that NUDT9 homologs are found only in multicellular eukaryotes suggests that vertebrates and possibly other multicellular eukaryotes possess mitochondrial metabolic processes that result in the production of free ADPR. Whether such processes are unique to multicellular eukaryotic mitochondria remains to be determined, although the presence of the highly specific ADPRase in *M. jannaschii* suggests that production of free ADP-ribose is not a unique feature of eukaryotic metabolism. In either case, the previous isolation of ADPRase activity from mitochondria, our cloning and characterization of NUDT9 as a specific ADPRase, and previous demonstrations of ADP-ribose production by isolated rat liver mitochondria provide a strong argument that ADP-ribose production in mitochondria is a physiologically important phenomenon in multicellular eukaryotes (21, 22). At present the role (if any) of free ADP-ribose produced by mitochondria in intact cell physiology or pathophysiology is currently unclear. An intriguing possibility, raised by our present results and our previous demonstration that the TRPM2 ion channel is gated by ADPR, is that mitochondrial production of ADP-ribose serves as a signaling mechanism for inducing the entry of extracellular Na and Ca via gating of TRPM2.

Acknowledgements—We thank Tomohiro Kurosaki for use of samples of the DT-40 cell cDNA library used to obtain chicken NUDT9 sequence by degenerate PCR. We also thank Angela Norbeck and Phil Gafken of the Proteomics Facility at Fred Hutchinson Cancer Center for mass spectrometry analyses and Debra A. McMillen at the Biotechnology Laboratory in the Institute of Molecular Biology at the University of Oregon, Eugene, OR, for N-terminal peptide sequencing.

REFERENCES

1. Perraud, A. L., Fleig, A., Dunn, C. A., Bagley, L. A., Launay, P., Schmitz, C., Stokes, A. J., Zhu, Q., Bessman, M. J., Penner, R., Kinet, J. P., and Scharenberg, A. M. (2001) *Nature* **411**, 595–599
2. Lin, S., Gasmi, L., Xie, Y., Ying, K., Gu, S., Wang, Z., Jin, H., Chao, Y., Wu, C., Zhou, Z., Tang, R., Mao, Y., and McLennan, A. G. (2002) *Biochim. Biophys. Acta* **1594,** 127–135
3. Jacobson, E. L., Cervantes-Laurean, D., and Jacobson, M. K. (1997) *Adv. Exp. Med. Biol.* **419,** 371–379
4. Ribeiro, J. M., Carloto, A., Costas, M. J., and Cameselle, J. C. (2001) *Biochim. Biophys. Acta* **1526,** 86–94
5. Dunn, C. A., O'Handley, S. F., Frick, D. N., and Bessman, M. J. (1999) *J. Biol. Chem.* **274,** 32318–32324
6. Canales, J., Pinto, R. M., Costas, M. J., Hernandez, M. T., Miro, A., Bernet, D., Fernandez, A., and Cameselle, J. C. (1995) *Biochim. Biophys. Acta* **1246,** 167–177
7. Bernet, D., Pinto, R. M., Costas, M. J., Canales, J., and Cameselle, J. C. (1994) *Biochem. J.* **299,** 679–682
8. Yang, H., Slupska, M. M., Wei, Y. F., Tai, J. H., Luther, W. M., Xia, Y. R., Shih, D. M., Chiang, J. H., Baikalov, C., Fitz-Gibbon, S., Phan, I. T., Conrad, A., and Miller, J. H. (2000) *J. Biol. Chem.* **275,** 8844–8853
9. Rippe, K., Mücke, N., and Schulz, A. (1998) *J. Mol. Biol.* **278,** 915–933
10. Stafford, W. F. (1992) *Anal. Biochem.* **203,** 295–301
11. Stafford, W. F. (1997) *Curr. Opin. Biotechnol.* **8,** 14–24
12. Philo, J. S. (2000) *Anal. Biochem.* **279,** 151–163
13. Gasmi, L., Cartwright, J. L., and McLennan, A. G. (1999) *Biochem. J.* **344,** 331–337
14. Sheikh, S., O'Handley, S. F., Dunn, C. A., and Bessman, M. J. (1998) *J. Biol. Chem.* **273,** 20924–20928
15. McLennan, A. G. (1999) *Int. J. Mol. Med.* **4,** 79–89
16. Bessman, M. J., Frick, D. N., and O'Handley, S. F. (1996) *J. Biol. Chem.* **271,** 25059–25062
17. Gabelli, S. B., Bianchet, M. A., Bessman, M. J., and Amzel, L. M. (2001) *Nat. Struct. Biol.* **8,** 467–472
18. Miro, A., Costas, M. J., Garcia-Diaz, M., Hernandez, M. T., and Cameselle, J. C. (1989) *FEBS Lett.* **244,** 123–126
19. Frick, D. N., Weber, D. J., Abeygunawardana, C., Gittis, A. G., Bessman, M. J., and Mildvan, A. S. (1995) *Biochemistry* **34,** 5577–5586
20. Harris, T. K., Wu, G., Massiah, M. A., and Mildvan, A. S. (2000) *Biochemistry* **39,** 1655–1674
21. Lotscher, H. R., Winterhalter, K. H., Carafoli, E., and Richter, C. (1980) *J. Biol. Chem.* **255,** 9325–9330
22. Richter, C., Gogvadze, V., Laffranchi, R., Schlapbach, R., Schweizer, M., Suter, M., Walter, P., and Yaffee, M. (1995) *Biochim. Biophys. Acta* **1271,** 67–74